CrystEngComm

ROYAL SOCIETY OF CHEMISTRY

PAPER

View Article Online
View Journal | View Issue

Cite this: *CrystEngComm*, 2026, **28**, 2455

Preparation of phosphine oxides with anthrylphenyl, pyrenylphenyl, anthrylethynyl, and pyrenylethynyl groups: luminescence properties and conformational polymorphs

Ryunosuke Konno,[a] Manami Fujita,[b] Rima Maekawa,[b] Hyuma Masu[c] and Kosuke Katagiri *[ab]

Received 29th August 2025,
Accepted 11th March 2026

DOI: 10.1039/d5ce00837a

rsc.li/crystengcomm

Precise control of crystal polymorphism provides a powerful strategy to tune luminescence, yet remains a major challenge in molecular material design. We show that introducing ethynylene linkers into phosphine oxide derivatives bearing anthryl and pyrenyl groups enables polymorphism through diverse intermolecular interactions, whereas phenylene-bridged analogues crystallize in a single form. Single-crystal X-ray diffraction confirmed distinct packing arrangements, and optical studies revealed extended π-conjugation with bathochromic shifts, as well as packing-dependent modulation of excited-state vibrational levels. These results establish a direct structure–property relationship between polymorphism and emission, offering a versatile molecular design principle for next-generation optoelectronic and photonic materials.

1. Introduction

The design of luminescent organic materials with tunable emission color and high stability has attracted sustained attention owing to their potential applications in organic light-emitting diodes, optical sensors, and bioimaging.[1,2] Among various candidates, lanthanide complexes coordinated with triphenylphosphine oxide (TPPO) are well-known examples,[3] where TPPO acts as an antenna molecule to enhance emission efficiency.[4] Previous studies have demonstrated that replacing the phenyl group of TPPO with extended π-conjugated substituents[5] such as anthryl[6] and pyrenyl[7] units can further improve light-harvesting capability and luminescence intensity, highlighting the significance of molecular design in tailoring photophysical properties.[8] Recently, increasing emphasis has been placed on controlling the luminescence of organic solids,[9] where the molecular packing in the crystal lattice is a decisive factor. Subtle variations in weak intermolecular interactions, including π–π stacking, CH–π, and halogen bonding, can fine-tune the emission color and efficiency. However, precise control of such interactions remains difficult, and the relationship between crystal packing and luminescence is not yet fully understood. One promising concept to address this challenge is crystal polymorphism,[10] in which a compound crystallizes in different packing motifs while maintaining the same chemical composition.[11] Polymorphism is well recognized for inducing significant changes in physical properties, and in luminescent systems, it provides a pathway to regulate solid-state emission. While strong hydrogen-bonding interactions often fix molecular arrangements into predictable patterns,[12] systems governed by multiple weak interactions are more likely to generate diverse crystal structures, thereby increasing the probability of polymorphism.[13] In this context, phosphine oxide derivatives bearing anthryl and pyrenyl substituents present an attractive platform for studying structure–property correlations in luminescent materials. These aromatic groups are expected to promote π–π stacking interactions, leading to diverse molecular arrangements. Furthermore, the introduction of an ethynylene linker between the phosphine oxide backbone and the aromatic substituent not only extends the π-conjugation, but also enhances rotational flexibility, which could significantly influence the diversity of crystal packing. This structural feature is therefore anticipated to promote polymorphism and, consequently, provide new opportunities for tuning luminescence behavior in the solid state. Herein, we report the design and synthesis of four phosphine oxide derivatives—9-anthrylphenyl, 9-anthrylethynyl, 1-pyrenylphenyl, and 1-pyrenylethynyl compounds (Chart 1)—to systematically investigate the effect

[a] *Graduate School of Natural Science, Konan University, 8-9-1 Okamoto, Higashinada-ku, Kobe 658-8501, Japan*
[b] *Department of Chemistry, Faculty of Science and Engineering, Konan University, 8-9-1 Okamoto, Higashinada-ku, Kobe 658-8501, Japan.*
E-mail: katagiri@konan-u.ac.jp
[c] *Center for Analytical Instrumentation, Chiba University, 1-33, Yayoi-cho, Inage-ku, Chiba 263-8522, Japan*

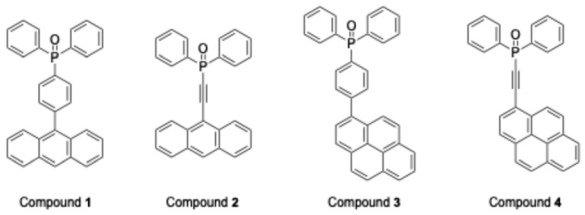

Chart 1 Chemical structures of the aryldiphenylphosphine oxides.

of ethynylene linkers on crystal packing and luminescence properties. Single-crystal X-ray diffraction analysis was performed under various recrystallization conditions to assess polymorph formation. In addition, the photophysical properties were examined in both solution and crystalline states, and the results were correlated with structural features. This study demonstrates how the incorporation of ethynylene groups into phosphine oxide frameworks can promote crystal polymorphism and provides a molecular design strategy for fine-tuning solid-state luminescence.

2. Experimental

2.1. Materials and instruments

All commercially available reagents were used without further purification. ^{1}H, ^{13}C, and ^{31}P nuclear magnetic resonance (NMR) spectra were recorded using an Agilent UNITY INOVA 500 spectrometer (500 MHz for ^{1}H, 126 MHz for ^{13}C, and 200 MHz for ^{31}P). Mass spectral data were obtained using a JEOL JMS-T100LP mass spectrometer in the positive-ion detection mode. Single crystal X-ray diffraction (SCXRD) data for crystals **1**, **2a**, **2b**, **3a**, **3c**, and **4** were collected on a RIGAKU Oxford Diffraction XtaLAB Pro equipped with a Dectris PILATUS 200K HPAD detector and microfocus sealed tube CuKα radiation with mirror optics (λ = 1.54184 Å). The diffraction data were integrated using CrysAlisPro[14] and corrected for absorption effects using a combination of empirical (ABSPACK) and numerical corrections. The structures were solved using SHELXT and refined by full-matrix least-squares analysis (SHELXL) using the OLEX2 program package.[15] Unless otherwise indicated, all non-hydrogen atoms were refined anisotropically. All the hydrogen atom positions were constrained to ideal geometries and refined using fixed isotropic displacement parameters (in terms of the riding model). X-ray diffraction images for crystals **1** and **2b** were collected using an EIGER 4M detector with synchrotron radiation at a wavelength of 0.80000 Å at the BL26B1 station of SPring-8 (Hyogo, Japan). The distance between the crystal and detector was 50 mm. Images were processed using HKL2000 (HKL Research) or the XDS program package. The structural solution and refinement were performed using SHELXS-97 and SHELXL-2014/7 (Sheldrick).[16,17] Powder X-ray diffraction (PXRD) patterns were recorded on a Bruker EMPYREAN diffractometer equipped with a CuKα radiation source (λ = 1.54184 Å) operating at 45 kV and 40 mA. The data were collected in the range of 2θ = 5–50° with a step size of 0.02° and a scanning speed of 4° min^{-1}. Ultraviolet-visible (UV-vis) spectra were recorded using a JASCO model V650 spectrophotometer. Fluorescence spectra were recorded using a JASCO FP8050 spectrophotometer (in solution) and JASCO FP8600 (in solid). Photoluminescence quantum yields (PQLYs) were obtained on a HAMAMATSU Photonics K.K. Quantaurus-QY C11347-01 series with an integrating sphere. All theoretical calculations were performed using the Gaussian 09 package,[18] details of which are given in the SI.

2.2. Synthesis procedure

2.2.1. Synthesis of (4-(9-anthryl)phenyl)diphenylphosphine oxide (compound 1). Under a N_2 atmosphere, 9-(4-bromophenyl)anthracene (0.359 g, 1.08 mmol) was dissolved in anhydrous tetrahydrofuran (12 mL). The solution was cooled to −78 °C, and *n*-BuLi was added (1.52 M in *n*-hexane, 1.5 mL, 2.3 mmol). After stirring for 30 min, chlorodiphenylphosphine (0.28 mL, 1.5 mmol) was added to the mixture and allowed to react at room temperature for 3 h. Subsequently, water was incorporated to deactivate any residual *n*-BuLi. Thereafter, hydrogen peroxide (30%, 1 mL) was added, and the mixture was stirred for 30 min. After the complete reaction, the mixture was quenched with water, extracted with chloroform, and washed with brine. The organic layer was then dried over anhydrous Na_2SO_4 and evaporated under reduced pressure. The crude product was purified by silica gel column chromatography using $CHCl_3$ and $CHCl_3$/MeOH (3 : 1 v/v) as eluents. Compound **1** was obtained as a white solid (0.244 g, 50.0%). ^{1}H NMR (500 MHz, $CDCl_3$, 25 °C): δ 8.53 (s, 1H), 8.06 (d, J = 8.5 Hz, 2H), 7.89–7.81 (m, 6H), 7.63–7.54 (m, 10H), 7.48 (t, J = 7.0, 7.5 Hz, 2H), 7.38 (t, J = 7.5 Hz, 2H) ppm; ^{13}C NMR (126 MHz, $CDCl_3$, 25 °C): δ 142.9, 135.4, 132.9, 132.3–132.1, 131.6, 131.5, 131.3, 129.9, 128.7, 128.6, 128.4, 127.2, 126.3, 125.7, 125.2 ppm; ^{31}P NMR (200 MHz, $CDCl_3$, 25 °C): δ 29.3 ppm. The MS (ESI-TOF) m/z calculated for $C_{32}H_{24}OP$ was 455.15648. Found: 455.11788.

2.2.2. Synthesis of (9-anthrylethynyl)diphenylphosphine oxide (compound 2). Under a N_2 atmosphere, 9-ethynylanthracene (0.145 g, 0.731 mmol) was dissolved in anhydrous tetrahydrofuran (10 mL). The solution was cooled to −78 °C, and *sec*-BuLi was added (1.2 M in *n*-hexane, 1 mL, 1.2 mmol). After being stirred for 30 min, chlorodiphenylphosphine (0.14 mL, 0.76 mmol) was added to the mixture and allowed to react at room temperature for 2 h. Subsequently, water was incorporated to deactivate any residual *n*-BuLi. Thereafter, hydrogen peroxide (30%, 1.5 mL) was added, and the mixture was stirred for 40 min. After the complete reaction, the mixture was quenched with water, extracted with chloroform, and washed with brine. The organic layer was then dried over anhydrous Na_2SO_4 and evaporated under reduced pressure. The crude product was purified by silica gel column chromatography using hexane/EtOAc (1 : 1 v/v) as the eluent. Compound **2** was obtained as a yellow solid (0.215 g,

73.1%). ^{1}H NMR (500 MHz, $CDCl_3$, 25 °C): δ 8.55 (s, 1H), 8.44 (dd, J = 1.0, 8.5 Hz, 2H), 8.09–8.03 (m, 6H), 7.61–7.53 (m, 10H) ppm; ^{13}C NMR (126 MHz, $CDCl_3$, 25 °C): δ 133.9, 133.8, 132.8, 132.4, 131.1, 130.8, 129.0, 128.8, 128.0, 126.0, 113.1, 103.2, 94.4, 93.1 ppm; ^{31}P NMR (200 MHz, $CDCl_3$, 25 °C): δ 8.40 ppm. The MS (ESI-TOF) m/z value calculated for $C_{28}H_{20}OP$ was 403.12518. Found: 403.14830.

2.2.3. Synthesis of (4-(1-pyrenyl)phenyl)diphenylphosphine oxide (compound 3). A mixture of (4-bromophenyl) diphenylphosphine oxide (0.360 g, 1.01 mmol), 1-pyreneboronic acid (0.502 g, 2.04 mmol), $Pd(PPh_3)_4$ (0.123 g, 0.106 mmol), and K_2CO_3 aq. (0.687 g, 4.97 mmol) in toluene/MeOH (v/v = 8 mL/2 mL) was refluxed under N_2 at 110 °C overnight. After cooling to room temperature, the mixture was filtered through Celite, quenched with water, extracted with chloroform, and washed with brine. The organic layer was then dried over anhydrous Na_2SO_4, and evaporated under reduced pressure. The crude product was purified by silica gel column chromatography using $CHCl_3$/EtOAc (20 : 1 v/v) as the eluent. Compound **3** was obtained as a light-brown solid (0.303 g, 62.9%). ^{1}H NMR (500 MHz, $CDCl_3$, 25 °C): δ 8.26–8.20 (m, 3H), 8.15–8.11 (m, 3H), 8.10–8.03 (m, 2H), 7.98 (d, J = 8.0 Hz, 1H), 7.90–7.80 (m, 6H), 7.76 (dd, J = 2.5 Hz, 2H), 7.62 (td, J = 1.5, 0.2, 1.5 Hz, 2H), 7.55 (td, J = 3.0, 4.0 Hz, 4H) ppm; ^{13}C NMR (126 MHz, $CDCl_3$, 25 °C): δ 145.0, 136.2, 133.0, 132.2, 132.1, 131.4, 131.0, 130.9, 130.8, 130.7, 128.7, 128.6, 128.4, 127.9, 127.8, 127.4, 126.2, 125.4, 125.1, 124.9, 124.8, 124.7, 124.7 ppm; ^{31}P NMR (200 MHz, $CDCl_3$, 25 °C): δ 29.2 ppm. MS (ESI-TOF): m/z calcd for $C_{34}H_{24}OP$: 479.15648. Found: 479.13168.

2.2.4. Synthesis of (1-pyrenylethynyl)diphenylphosphine oxide (compound 4). Under a N_2 atmosphere, 1-ethynylpyrene (0.141 g, 0.623 mmol) was dissolved in anhydrous tetrahydrofuran (10 mL). The solution was cooled to −78 °C, and *sec*-BuLi was added (1.2 M in *n*-hexane, 0.7 mL, 0.8 mmol). After being stirred for 30 min, chlorodiphenylphosphine (0.14 mL, 0.76 mmol) was added to the mixture and allowed to react at room temperature for 2 h. Subsequently, water was incorporated to deactivate any residual *n*-BuLi. Thereafter, hydrogen peroxide (30%, 1.5 mL) was added, and the mixture was stirred for 30 min. After the complete reaction, the mixture was quenched with water, extracted with chloroform, and washed with brine. The organic layer was then dried over anhydrous Na_2SO_4, and evaporated under reduced pressure. The crude product was purified by silica gel column chromatography using hexane/EtOAc (20 : 1, 10 : 1, 1 : 1 v/v) as the eluent. Compound **4** was obtained as a yellow solid (0.244 g, 91.9%). ^{1}H NMR (500 MHz, $CDCl_3$, 25 °C): δ 8.48 (d, J = 9.5 Hz, 1H), 8.26–8.24 (m, 3H), 8.20–8.16 (m, 2H), 8.13 (d, J = 8.0 Hz, 1H), 8.10–8.03 (m, 6H), 7.62–7.59 (m, 2H), 7.58–7.54 (m, 4H) ppm; ^{13}C NMR (126 MHz, $CDCl_3$, 25 °C): δ 133.8, 133.2, 132.9, 132.8, 132.3, 131.1, 131.0, 130.7, 130.4, 128.8, 128.7, 127.1, 126.6, 126.4, 124.7, 124.4, 124.1, 123.9, 113.6, 105.2, 88.8, 87.5 ppm; ^{31}P NMR (200 MHz, $CDCl_3$, 25 °C): δ 8.46 ppm. The MS (ESI-TOF) m/z calculated for $C_{30}H_{20}OP$ was 427.12518. Found: 427.11886.

3. Results and discussion

3.1. Synthesis

Phenylene-bridged triarylphosphine oxide derivatives **1** and **3** were synthesized by two distinct methodologies. In the first approach, 4-anthrylbromobenzene was obtained through a Suzuki cross-coupling reaction between 4-iodobromobenzene and anthracene boronic acid. Subsequent halogen–lithium exchange, followed by reaction with chlorodiphenylphosphine and oxidation with hydrogen peroxide, furnished compound **1** in 50% yield (Scheme S1). This procedure, however, failed to afford compound **3** in a pure form. In an alternative approach, 4-halophenyldiphenylphosphine oxide was initially prepared, and subsequent Suzuki cross-coupling with pyrenyl moieties afforded compound **3** in 63% yield (Scheme S2). Application of this methodology to the synthesis of compound **1** was hampered by difficulties associated with separation of by-products. Ethynylene-bridged analogues **2** and **4** were synthesized by three different routes. In the first route, ethynyldiphenylphosphine oxide was prepared and subjected to Sonogashira cross-coupling with 9-bromoanthracene and 1-bromopyrene (Scheme S3). In the second route, 9-haloanthracene and bromopyrene were coupled with trimethylsilylacetylene to afford ethynylanthracene and ethynylpyrene, respectively. The resulting intermediates were converted to the corresponding acetylide anions by treatment with butyllithium, which were subsequently reacted with chlorodiphenylphosphine and oxidized with hydrogen peroxide to yield the target compounds (Scheme S4). In the third route, ethynylanthracene and ethynylpyrene were prepared from the corresponding aldehydes *via* the Corey–Fuchs reaction.[19] The resulting intermediates were subjected to the same sequence of transformations as in the second route to furnish the desired products (Scheme S5). While both Sonogashira-based methodologies failed to provide analytically pure products, the Corey–Fuchs route[18] afforded

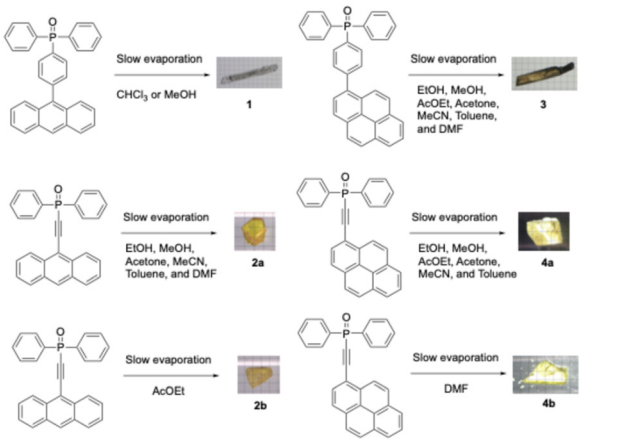

Scheme 1 Crystallization conditions.

compounds **2** and **4** in isolated yields of 54% and 92%, respectively, over four steps (Scheme 1).

3.2. Crystal structures

The four synthesized phosphine oxide compounds were recrystallized in various solvents, including chloroform, ethyl acetate, tetrahydrofuran (THF), *N*,*N*-dimethylformamide (DMF), methanol, and toluene. A single crystal was obtained by dissolving 5 mg of the compound in a solvent (0.5 mL); the mixture was heated and allowed to stand at room temperature. This crystal was then analyzed *via* SCXRD to identify its crystal structure (Fig. 1). The following scheme shows the correlation between the phosphine oxide crystallization conditions and the resulting crystal structures.

3.2.1. (4-(9-Anthryl)phenyl)diphenylphosphine oxide 1. Single crystals suitable for single-crystal X-ray diffraction (SCXRD) analysis were obtained from chloroform/methanol mixed solutions. The pale-yellow crystals crystallize in the monoclinic system with the space group $P2_1/n$. The anthryl substituent is attached at the 4-position of one of the three phenyl groups of the phosphine oxide core. In the solid state, the molecules are organized into a one-dimensional (1D) chain structure through C–H···π interactions between the anthryl unit and the phenyl rings of adjacent molecules (Fig. 2a). Additional C–H···π interactions involving the anthryl hydrogen atoms and neighboring phenyl groups extend this arrangement into a two-dimensional (2D) layer (Fig. 2b and c). The dihedral angle between the planes of the anthryl and phenylene units was determined to be 71.6°, clearly indicating that these moieties are not coplanar in the crystal structure (Fig. 2d). Hirshfeld surface analysis was performed to visualize intermolecular contacts (Fig. 2e). In the mapped surface, regions corresponding to hydrogen-bonding appear in red, reflecting relatively strong interactions. The contribution of C–H contacts to the overall intermolecular interactions was calculated to be 40.9% (Fig. 2f), suggesting a predominance of weak interactions among the multiple aromatic rings.

3.2.2. (9-Anthrylethynyl)diphenylphosphine oxide 2a. Compound **2** was recrystallized from mixed solvents to afford single crystals (**2a**) suitable for SCXRD analysis. The pale-yellow crystals crystallize in the monoclinic system with the space group $P2_1/c$. In the molecular structure, the ethynylanthryl substituent is bound to the oxadiphenylphosphino moiety. Within the crystal packing, hydrogen bonds between the phenyl and oxophosphino groups organize the molecules into a zigzag one-dimensional (1D) chain along the *c*-axis (Fig. 3a). Additional C–H···π interactions between the anthryl unit of the ethynyl substituent and phenyl rings of adjacent molecules extend the packing into a two-dimensional (2D) layer along the *b*-axis (Fig. 3b and c). Furthermore, π–π interactions between anthryl units of neighboring molecules were also identified (Fig. 3b). The ethynyl moiety, typically expected to exhibit a linear geometry with a bond angle of 180°, was found to be significantly bent in the crystal structure (∠P–C–C = 164.5°, ∠C–C–C = 175.9°; Fig. 3d). Hirshfeld surface analysis was carried out to visualize intermolecular interactions (Fig. 3e). Regions corresponding to hydrogen-bonding and C–H···π contacts appear in red, reflecting relatively strong interactions. The contribution of C–H contacts to the overall intermolecular interactions was calculated to be 38.8%

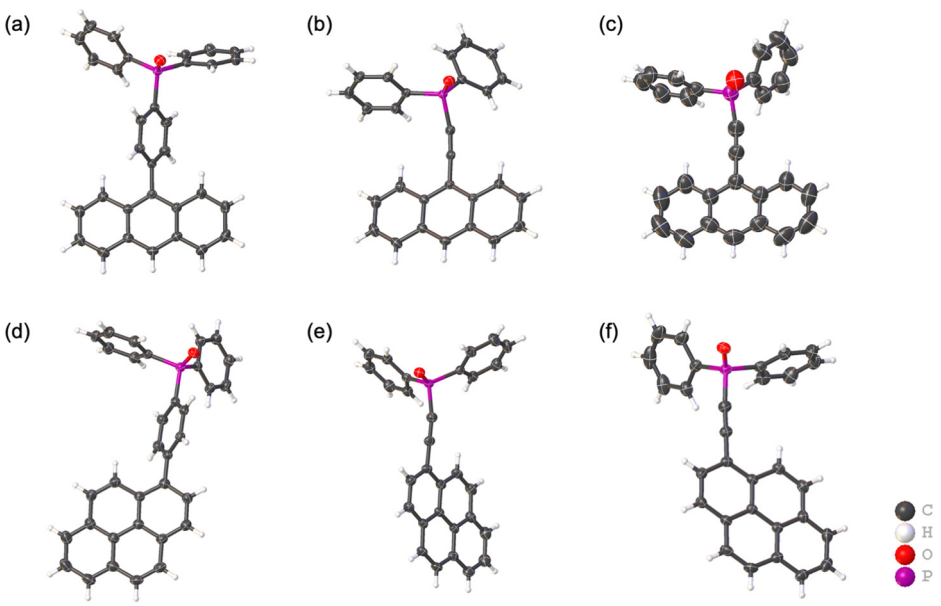

Fig. 1 Crystal structures of (a) (4-(9-anthryl)phenyl)diphenylphosphine oxide **1**, (b) (9-anthrylethynyl)diphenylphosphine oxide **2a**, (c) (9-anthrylethynyl)diphenylphosphine oxide **2b**, (d) (4-(1-pyrenyl)phenyl)diphenylphosphine oxide **3**, (e) (1-pyrenylethynyl)diphenylphosphine oxide **4a**, and (f) (1-pyrenylethynyl)diphenylphosphine oxide **4b** in the thermal ellipsoid model. The ellipsoids of all non-hydrogen atoms have been drawn at the 50% probability level.

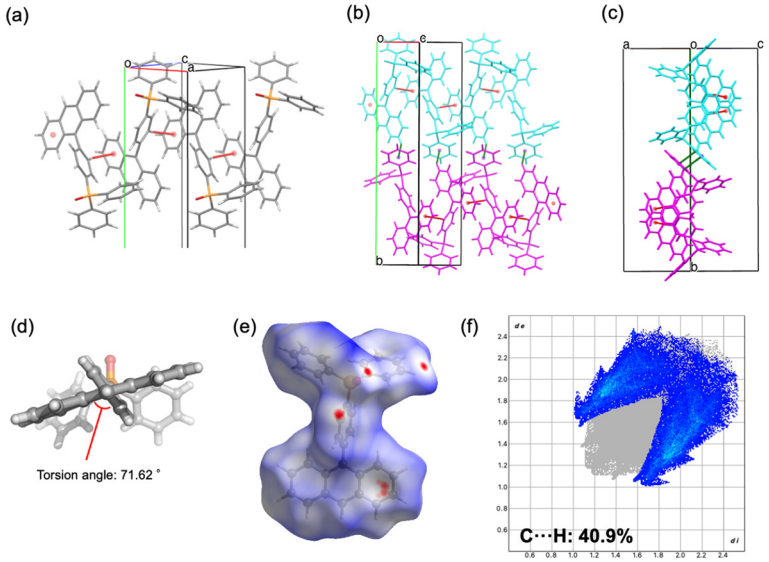

Fig. 2 Compound **1**. (a) 1D linear chain of **1** *via* CH/π interactions. The CH/π interactions are shown in red color. (b) 2D layer network *via* CH/π interactions (top view). The CH/π interactions are shown in green color. (c) 2D layer network *via* CH/π interactions (side view). The CH/π interactions are shown in green color. (d) Dihedral angle between the planes formed by an anthryl group and a phenylene group of **1**. (e) Hirshfeld surface mapped with d_{norm} for **1**. (f) Fingerprint plot for **1**.

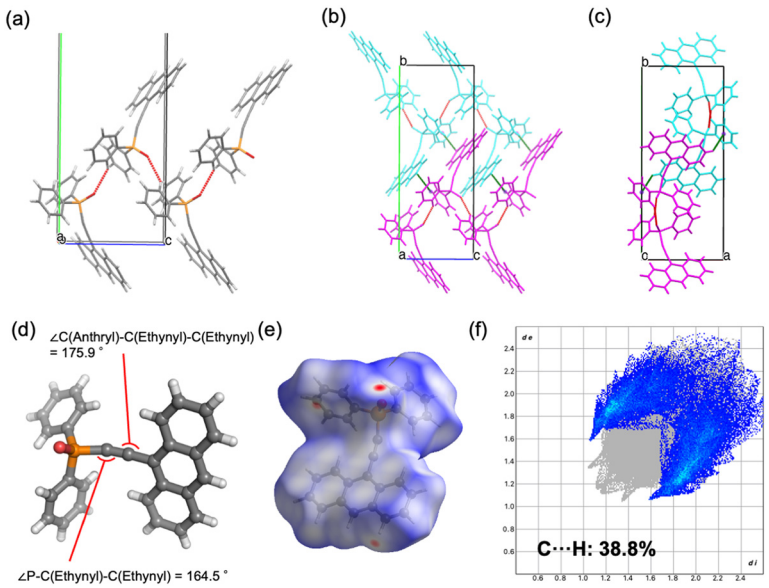

Fig. 3 Compound **2a**. (a) 1D zigzag chain of **2a** *via* P═O···H interactions. The P═O···H interactions are shown in red color. (b) 2D layer network *via* CH/π interactions (top view). The CH/π interactions are shown in green color. (c) 2D layer network *via* CH/π interactions (side view). The CH/π interactions are shown in green color. (d) Bond angles of the ethynyl group. (e) Hirshfeld surface mapped with d_{norm} for **2a**. (f) Fingerprint plot for **2a**.

(Fig. 3f), indicating a predominance of weak aromatic interactions in the crystal lattice.

3.2.3. (9-Anthrylethynyl)diphenylphosphine oxide 2b. Single crystals of **2b** suitable for SCXRD analysis were obtained from ethyl acetate solutions. The pale-yellow crystals represent a polymorphic form of **2a** and crystallize in the triclinic system with the space group $P\bar{1}$. The molecular structure is identical to that of **2a**, consisting of an ethynylanthryl substituent attached to the oxadiphenylphosphino moiety. In the crystal packing, two phosphine oxide molecules form a dimer through C–H···O hydrogen bonding between a phenyl hydrogen atom and the oxygen atom of the oxophosphino group (Fig. 4a). These dimers assemble into one-dimensional (1D) chains along the *b*-axis, mediated by additional C–H···π interactions between phenyl groups (Fig. 4b). Weak π–π interactions between the anthryl units of adjacent dimers

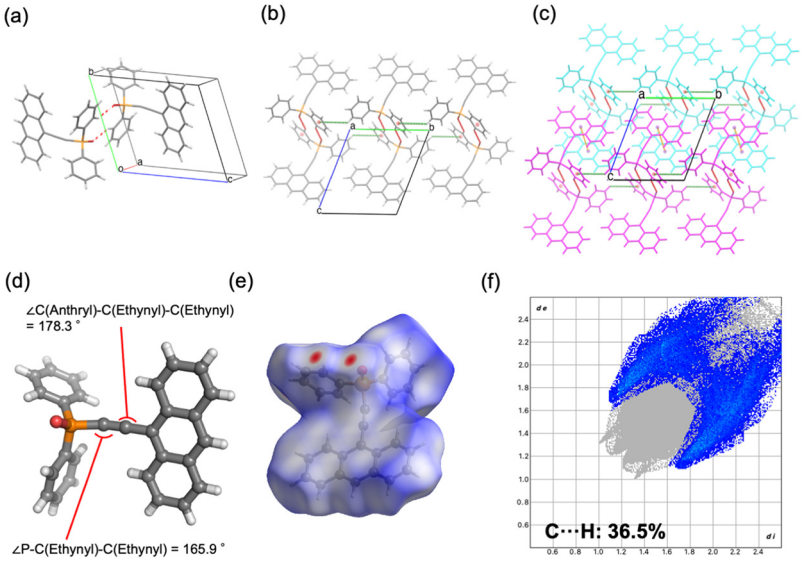

Fig. 4 Compound **2b**. (a) Dimer of **2b** *via* P═O···H interactions. The P═O···H interactions are shown in red color. (b) 1D chain network *via* CH/π interactions. The CH/π interactions are shown in green color. (c) 2D layer network *via* π/π interactions. The π/π interactions are shown in orange color. (d) Bond angles of the ethynyl group. (e) Hirshfeld surface mapped with d_{norm} for **2b**. (f) Fingerprint plot for **2b**.

align the 1D chains into a parallel arrangement (Fig. 4c). The centroid–centroid distance between the anthryl moieties was determined to be 3.880 Å. The ethynyl group displayed a geometry closer to linearity compared to polymorph **2a**, with bond angles of ∠P–C–C = 165.9° and ∠C–C–C = 178.3° (Fig. 4d). Hirshfeld surface analysis was conducted to further examine intermolecular interactions (Fig. 4e). In the surface mapping, regions corresponding to hydrogen bonds are highlighted in red, whereas C–H···π and π–π interactions appear in white, suggesting interaction strengths comparable to van der Waals forces. The contribution of C–H···π contacts was calculated to be 36.5% (Fig. 4f), indicating a lower proportion of weak aromatic interactions relative to polymorph **2a**.

3.2.4. (4-(1-Pyrenyl)phenyl)diphenylphosphine oxide 3. Single crystals of **3** suitable for SCXRD analysis were obtained from chloroform/methanol mixed solutions. The pale-yellow crystals crystallize in the monoclinic system with the space group $P2_1/c$. The molecular structure consists of a pyrenyl substituent attached to the 4-position of one of the three phenyl groups of the phosphine oxide core. In the crystal packing, molecules assemble into a one-dimensional (1D)

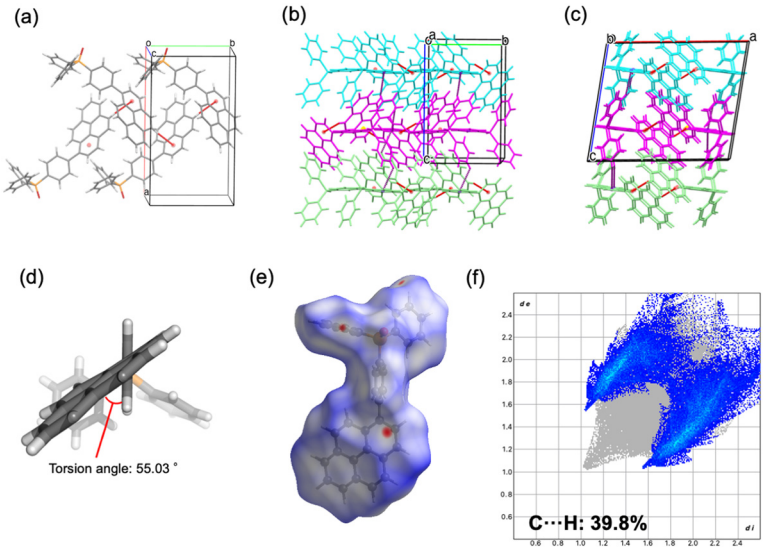

Fig. 5 Compound **3**. (a) 1D linear chain of **3** *via* CH/π interactions. The CH/π interactions are shown in red color. (b) 2D layer network *via* CH/π interactions (top view). The CH/π interactions are shown in purple color. (c) 2D layer network *via* CH/π interactions (side view). The CH/π interactions are shown in purple color. (d) Dihedral angle between the plane formed by an anthryl group and the plane formed by a phenylene group of **3**. (e) Hirshfeld surface mapped with d_{norm} for **3**. (f) Fingerprint plot for **3**.

chain along the *b*-axis through C–H···π interactions between pyrenyl moieties of adjacent molecules (Fig. 5a). Additional C–H···π interactions between phenyl groups extend this arrangement along the *c*-axis, resulting in a two-dimensional (2D) layered structure (Fig. 5b and c). The dihedral angle between the planes of the pyrenyl and phenylene groups was determined to be 54.3°, confirming their non-coplanarity in the solid state (Fig. 5d). Hirshfeld surface analysis was performed to visualize intermolecular interactions (Fig. 5e). Regions corresponding to C–H···π contacts are highlighted in white, indicative of relatively strong interactions. The contribution of C–H···π contacts to the overall intermolecular interactions was calculated to be 39.8% (Fig. 5f), suggesting that weak aromatic interactions play a predominant role in the packing arrangement.

3.2.5. (1-Pyrenylethynyl)diphenylphosphine oxide 4a. Recrystallization of **4** from mixed solvents afforded single crystals (**4a**) suitable for SCXRD analysis. The pale-yellow crystals crystallize in the monoclinic system with the space group $P2_1/c$. The molecular structure comprises an ethynylpyrenyl substituent bound to the oxadiphenylphosphino moiety. In the crystal packing, hydrogen bonds are formed between the phenyl and oxophosphino groups as well as between the pyrenyl and oxophosphino groups, generating a two-dimensional (2D) layered structure within the *ab* plane (Fig. 6a). Additional π–π interactions between pyrenyl moieties were also identified (Fig. 6b). The ethynyl unit adopts a geometry close to linearity, with bond angles of ∠P–C–C = 169.2° and ∠C–C–C = 179.1° (Fig. 6c), indicating a more linear configuration relative to compound **2**. Hirshfeld surface analysis was carried out to examine intermolecular contacts (Fig. 6d). Regions corresponding to hydrogen-bonding interactions are highlighted in red, while those associated with C–H···π interactions appear in white, suggesting interaction strengths comparable to van der Waals contacts. The contribution of C–H···π contacts to the overall intermolecular interactions was calculated to be 43.8% (Fig. 6e), reflecting the prevalence of weak aromatic interactions in the crystal lattice.

3.2.6. (1-Pyrenylethynyl)diphenylphosphine oxide 4b. Single crystals of **4b** suitable for SCXRD analysis were obtained from DMF solutions. The pale-yellow crystals represent a polymorphic form of **4a** and crystallize in the monoclinic system with the space group $P2_1/c$. In the crystal packing, hydrogen bonds are formed between the oxophosphino group and multiple positions of the pyrenyl unit (C–H at the 5,6-positions and the 3-position) as well as with phenyl groups, thereby generating a two-dimensional (2D) layered structure within the *ac* plane (Fig. 7a). In addition, intermolecular π–π interactions between pyrenyl groups were observed (Fig. 7b). The ethynyl unit adopts a nearly linear geometry, with bond angles of ∠P–C–C = 174.5° and ∠C–C–C = 178.8° (Fig. 7c), indicating a more linear structure relative to polymorph **4a**. Hirshfeld surface analysis was performed to examine intermolecular contacts (Fig. 7d). Regions corresponding to hydrogen-bonding interactions are highlighted in red, whereas those associated with π–π and C–H···π contacts appear in white, suggesting interaction strengths comparable to van der Waals forces. The contribution of C–H···π contacts to the overall interactions was calculated to be 36.9% (Fig. 7e), indicating reduced prevalence of weak aromatic interactions compared to polymorph **4a**.

3.2.7. Structural information and polymorphism. Crystal polymorphism refers to the occurrence of multiple solid-state arrangements for a given molecule. The likelihood of polymorphism is generally correlated with the number of potential hydrogen-bonding sites, halogen-bonding sites, and aromatic ring–ring interaction sites. Aromatic substituents

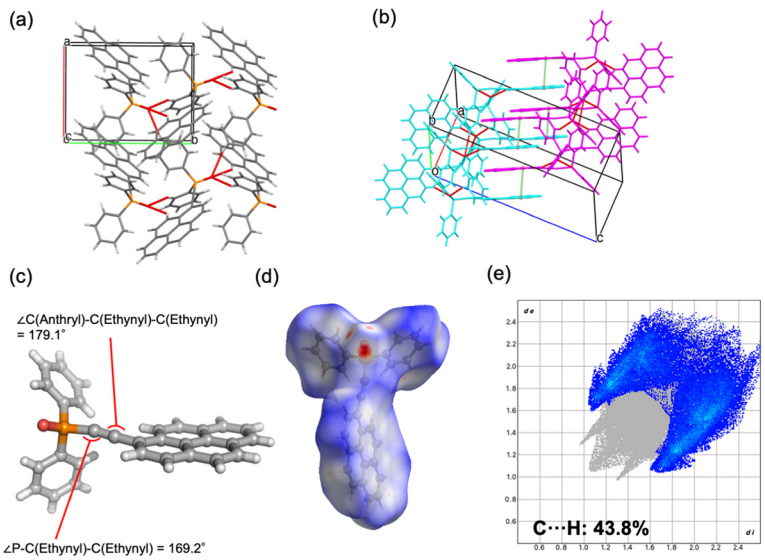

Fig. 6 Compound **4a**. (a) 2D layer of **4a** *via* P═O···H interactions. The P═O···H interactions are shown in red color. (b) 2D layer network *via* π/π interactions. The π/π interactions are shown in green color. (c) Bond angles of the ethynyl group. (d) Hirshfeld surface mapped with d_{norm} for **4a**. (e) Fingerprint plot for **4a**.

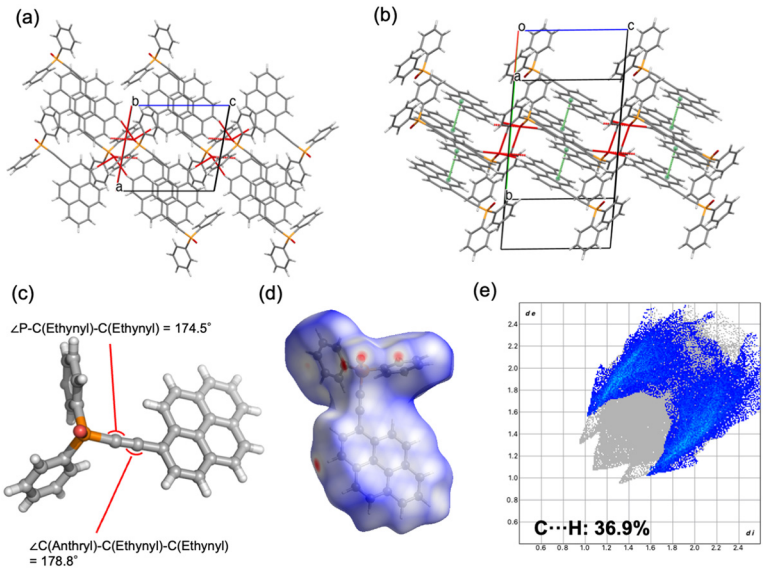

Fig. 7 Compound **4b**. (a) 2D layer of **4b** *via* P═O···H interactions. The P═O···H interactions are shown in red color. (b) 2D layer network *via* π/π interactions. The π/π interactions are shown in green color. (c) Bond angles of the ethynyl group. (d) Hirshfeld surface mapped with d_{norm} for **4b**. (e) Fingerprint plot for **4b**.

such as anthryl and pyrenyl units are therefore expected to promote intermolecular π–π interactions. In the phenylene-bridged compounds **1** and **3**, the dihedral angles between the phenylene group and anthryl and pyrenyl groups are 71° and 55°, respectively (Table S6). This twisted conformation stabilizes the structures, indicating a loss of planarity between the phenylene moiety and the anthryl or pyrenyl groups. Accordingly, no polymorphism was observed for the phenylene-bridged compounds **1** and **3** synthesized in this study under various recrystallization conditions. This absence is most likely attributable to the restricted rotational freedom of the anthryl and pyrenyl substituents, which effectively fix the molecular geometry and reduce the diversity of weak interaction sites. By contrast, polymorphism was unambiguously confirmed for the ethynylene-bridged compounds **2** and **4**, for which distinct crystalline forms were obtained depending on the recrystallization solvent (Fig. 8). This is thought to occur in the ethynylene-bridged type because the removal of torsion allows the anthryl and pyrenyl groups to rotate freely, thereby optimizing the interactions between the aromatic rings. The selected bond angles are summarized in Table S1. Furthermore, intermolecular

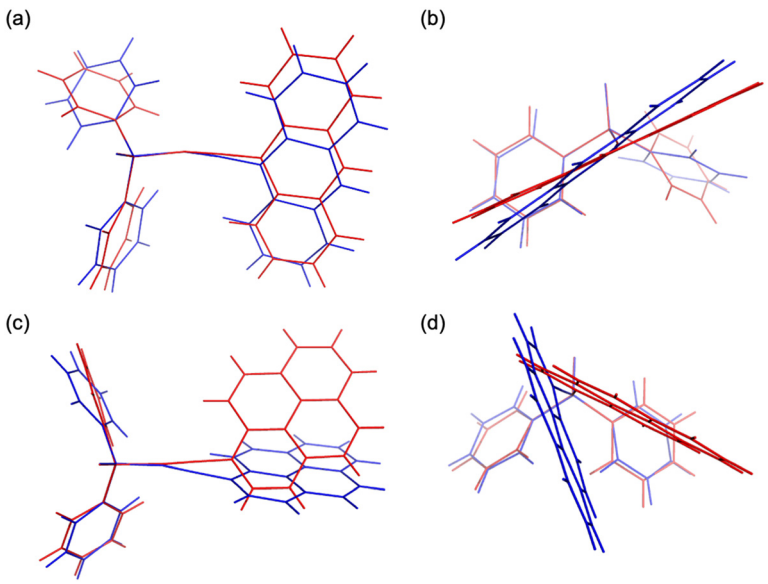

Fig. 8 Overlay of crystal polymorphs. (a) Top view of polymorphs **2a** (red) and **2b** (blue). (b) Side view of polymorphs **2a** (red) and **2b** (blue). (c) Top view of polymorphs **4a** (red) and **4b** (blue). (d) Side view of polymorphs **4a** (red) and **4b** (blue).

interaction energies calculated using Crystal Explorer revealed that ethynylene-bridged molecules form stronger interactions with adjacent molecules than phenylene-bridged analogues. Specifically, the strongest interaction in **1** was −71.6 kJ mol^{-1}, whereas those in **2a** and **2b** were −95.8 kJ mol^{-1} and −83.6 kJ mol^{-1}, respectively. Similarly, the strongest interaction in **3** was −39.6 kJ mol^{-1}, compared with −63.0 kJ mol^{-1} and −71.6 kJ mol^{-1} in **4a** and **4b**, respectively. The oxaphosphino group acts as a hydrogen bond acceptor in five of six crystals obtained. It exerts a strong influence on molecular arrangement and is considered to establish a structural framework that prevents excessive divergence of packing modes. The detailed structure of each polymorph is described below. In the case of compound **2**, polymorph **2a** (monoclinic, $P2_1/c$) exhibited zigzag one-dimensional chains stabilized by C–H···O and C–H···π interactions, whereas **2b** (triclinic, $P\bar{1}$) formed dimeric units through C–H···O hydrogen bonding, which further assembled into chains. The geometry of the ethynyl moiety was more linear in **2b** (∠P–C–C = 165.9°, ∠C–C–C = 178.3°) than in **2a** (164.5° and 175.9°). Hirshfeld surface analysis further demonstrated a reduced contribution of C–H···π contacts in **2b** (36.5%) compared to **2a** (38.8%), reflecting differences in the balance of weak aromatic interactions. For compound **4**, both polymorphs crystallized in the monoclinic system ($P2_1/c$), but with distinct packing motifs. Polymorph **4a** formed layered structures within the *ab* plane through hydrogen bonding involving both phenyl and pyrenyl moieties, whereas **4b** generated layers in the *ac* plane, stabilized by hydrogen bonding at multiple positions of the pyrenyl group. In both cases, π–π interactions between pyrenyl units contributed to the packing arrangement. The ethynyl moiety was again more linear in **4b** (∠P–C–C = 174.5°, ∠C–C–C = 178.8°) relative to **4a** (169.2° and 179.1°). Hirshfeld surface analysis revealed a lower proportion of C–H···π interactions in **4b** (36.9%) than in **4a** (43.8%), indicating reduced prevalence of weak aromatic contacts. Taken together, these results demonstrate that the conformational flexibility imparted by the ethynyl linkage, in contrast to the rigidity of the phenylene bridge, enables multiple packing modes in the solid state. The ability of the sp-hybridized ethynyl group to maintain a nominally linear geometry while tolerating slight distortions further augments the diversity of molecular arrangements, thereby increasing the probability of crystal polymorphism in compounds **2** and **4**.

3.3. Luminescence properties in solution state

Fig. 9 presents the UV-vis absorption spectra of the synthesized phosphine oxides in acetonitrile solution. For the anthryl-substituted derivatives, the phenylene-bridged compound **1** exhibited absorption bands at 348, 365, and 385 nm, with a maximum absorption at 365 nm. In contrast, the ethynylene-bridged compound **2** displayed absorption at 374, 393, and 415 nm, with the maximum absorption red-shifted

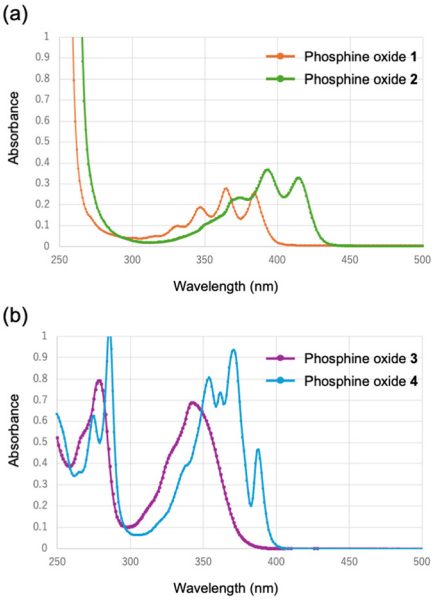

Fig. 9 UV-vis absorption spectra of (a) **1** (orange) and **2** (green), and (b) **3** (purple) and **4** (blue) in CH_3CN.

to 393 nm relative to **1**. A similar trend was observed for the pyrenyl-substituted compounds. The phenylene-bridged derivative **3** exhibited absorptions at 279 and 343 nm, with the most intense band at 279 nm. Conversely, the ethynylene-bridged compound **4** showed relatively sharp absorption features at 290, 357, 375, and 389 nm, with a maximum absorption at 375 nm, red-shifted relative to **3**. Thus, for both anthryl- and pyrenyl-containing derivatives, the ethynylene-bridged analogues consistently exhibited bathochromic shifts compared to their phenylene-bridged counterparts. This red-shift can be rationalized by the extended π-conjugation enabled by the ethynyl linkage, wherein the additional p-orbitals of the sp-hybridized carbon atoms contribute to delocalization. Notably, the absorption spectrum of **3** displayed significant broadening, indicative of enhanced electronic coupling between the pyrenyl, phenylene, and oxaphosphino moieties.

3.4. Fluorescence spectra in solution state

Fig. 10 displays the fluorescence spectra of the phosphine oxides in acetonitrile solution. Emission bands characteristic of anthracene were observed, with maxima in the 400–500 nm region, consistent with monomeric anthracene fluorescence reported in the literature. For the anthryl-substituted derivatives, the phenylene-bridged compound **1** exhibited an emission maximum at 420 nm, whereas the ethynylene-bridged compound **2** showed an emission maximum at 455 nm. This bathochromic shift is consistent with the absorption behavior and can be attributed to the extended π-conjugation introduced by the ethynyl linkage. In contrast, the pyrenyl-substituted derivatives displayed emission bands in the 374–410 nm region, which are

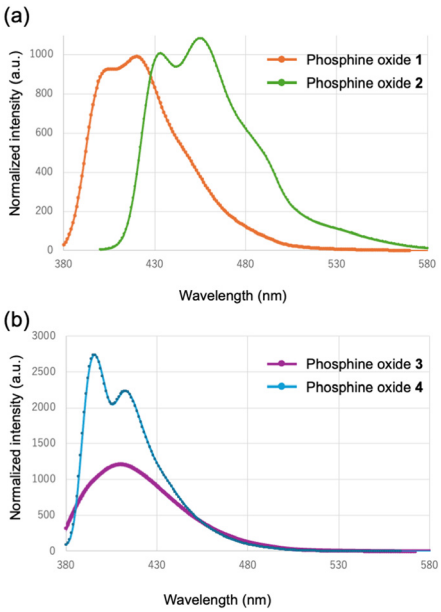

Fig. 10 Fluorescence spectra of (a) **1** (orange) and **2** (green), and (b) **3** (purple) and **4** (blue) in CH_3CN.

characteristic of monomeric pyrene fluorescence in solution. Specifically, the phenylene-bridged compound **3** displayed an emission at 410 nm, while the ethynylene-bridged compound **4** exhibited a maximum emission at 396 nm. These emission features are consistent with the locally excited state of pyrene monomers. Although the absorption spectra revealed red-shifts upon replacement of the phenylene unit with an ethynyl linker, the fluorescence wavelengths did not follow the same trend. Specifically, compound **3** displayed a longer emission wavelength than compound **4**. The broadening of the fluorescence spectrum of **3** suggests pronounced electron delocalization and intramolecular polarization, which likely contribute to the observed bathochromic shift relative to **4**.

3.5. Luminescence properties in solid state

Fig. 11 presents the UV-visible absorption spectra of the phosphine oxides in the solid state. Consistent with the solution-phase results, expansion of the conjugated system was confirmed by the conversion form the phenylene-bridged structure to the ethynylene-bridged structure. Specifically, the maximum absorption wavelengths of the ethynylene-bridged compounds **2** and **4** exhibited red shifts relative to the corresponding phenylene-bridged compounds **1** and **3**. Since both compounds **2** and **4** exhibit crystalline polymorphism, the absorption spectra of their respective polymorphs were compared; however, no significant differences were observed.

3.6. Fluorescence spectra in solid state

Fig. 12 depicts the solid-state fluorescence spectra of the synthesized phosphine oxides. For the anthryl-substituted derivatives, the maximum emission wavelengths were observed at 431 nm for the phenylene-bridged compound **1** and 433 nm for the ethynylene-bridged compound **2a**. These emission bands are characteristic of monomeric anthracene fluorescence in the solid state. Despite the red shift in absorption associated with conjugation extension, the emission wavelengths remained essentially unchanged, indicating that extension of π-conjugation does not significantly alter the nature of the emissive excited state in

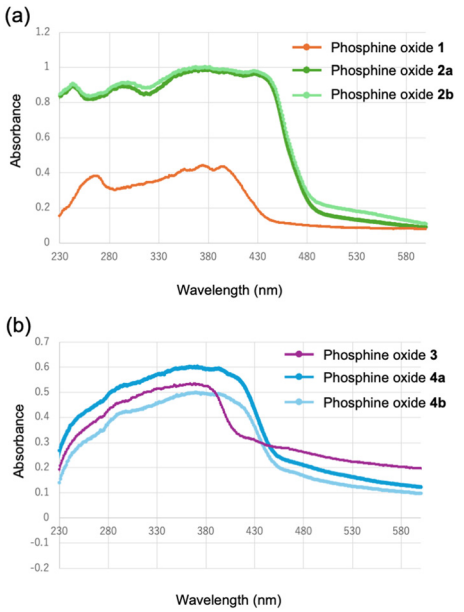

Fig. 11 UV-vis absorption spectra of (a) **1** (orange), **2a** (green), and **2b** (light green); (b) **3** (purple), **4a** (blue), and **4b** (light blue) in the solid state.

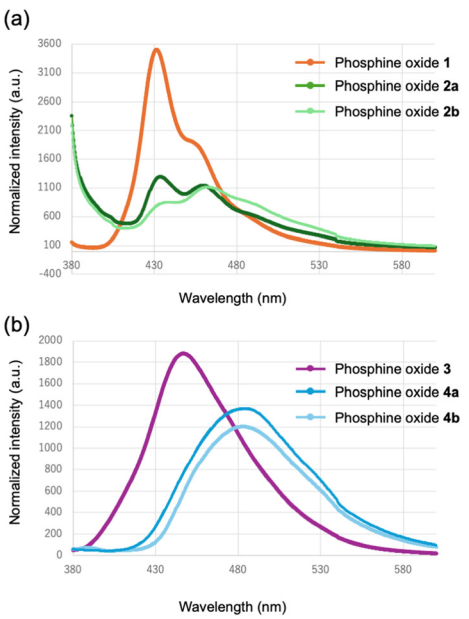

Fig. 12 Fluorescence spectra of (a) **1** (orange), **2a** (green), and **2b** (light green); (b) **3** (purple), **4a** (blue), and **4b** (light blue) in the solid state.

these crystalline forms. By contrast, the ethynylene-bridged polymorph **2b** exhibited a red-shifted maximum emission wavelength of 462 nm. This bathochromic shift and spectral broadening are indicative of excimer-like emission arising from enhanced π–π interactions between anthracene units in the crystal lattice. The observed dual-emission behavior in this system is therefore attributed to the coexistence of monomeric and excimer-like emissive states, which are stabilized differently depending on the molecular packing arrangement. These results suggest that variations in intermolecular interactions can modulate excited-state stabilization through packing-dependent electronic coupling. Although precise control of crystal polymorphism remains a considerable challenge, these findings imply that modulation of weak interactions—particularly those involving aromatic moieties—can subtly alter molecular packing and thereby enable fine-tuning of emission characteristics. In the case of pyrenyl-substituted derivatives, the maximum emission wavelengths were determined to be 446 nm for the phenylene-bridged compound **3**, 484 nm for the ethynylene-bridged compound **4a**, and 483 nm for crystalline polymorph **4b**. The emission bands in compounds **4a** and **4b**, which appear in the 480 nm region, are consistent with excimer-type emission typically observed for pyrene aggregates in the solid state. In contrast, emission in compound **3** contains a larger contribution from monomer-like fluorescence. Consistent with the absorption spectra (Fig. 9 and 11), the replacement of the phenylene bridge with an ethynylene unit extends the π-conjugated system. Nevertheless, in the pyrenyl series, this structural modification exerts negligible influence on the fluorescence maxima, underscoring the limited role of extended conjugation in modulating the emissive properties of pyrenyl-based phosphine oxides.

3.7. Photoluminescence quantum yields (PLQYs)

The PLQYs of the crystals, measured using an integrating sphere under deoxygenated conditions, were determined to be 51.4%, 6.7%, 0.8%, 45.6%, 47.7%, and 45.0% for crystals **1**, **2a**, **2b**, **3**, **4a**, and **4b**, respectively (Fig. S50–S55). Differences in crystal packing patterns modify intermolecular interactions and influence nonradiative decay pathways. In phenylene-bridged phosphine oxide **1**, π–π stacking interactions between molecules are absent, resulting in relatively weak intermolecular packing; consequently, monomer-like emission is expected. The PLQY of approximately 50% supports this interpretation. In contrast, π–π stacking interactions are observed in the ethynylene-bridged polymorphs **2a** and **2b**. The extremely low quantum yields suggest the presence of excimer-like interactions that facilitate nonradiative decay. For phosphine oxides bearing pyrene moieties, nonradiative relaxation appears to be suppressed in both the phenylene-bridged and ethynylene-bridged derivatives, with only minimal reductions in PLQY observed. These results indicate that the presence of extended π–π interactions can significantly promote nonradiative pathways, particularly in the anthryl-containing systems.

3.8. Theoretical calculations

Quantum mechanical calculations were performed at the B3LYP/6-31g(d) level of theory to gain further insight into the structural and electronic properties of the crystals. Structural optimization was carried out using density functional theory (DFT) based on the geometries obtained from single-crystal X-ray diffraction data. Excited states were subsequently calculated with time-dependent DFT (TD-DFT) at the same level of theory, employing the optimized geometries. The optimized molecular geometries, HOMO and LUMO energy levels, and the corresponding frontier orbital distributions are shown in Fig. S56. Conversion from phenylene-bridged to ethynylene-bridged structures extends the π-conjugated system, leading to a red shift in the absorption wavelength. This interpretation is supported by the computational results, which show that the HOMO–LUMO gaps of the ethynylene-bridged species (**2a**, **2b**, **4a** and **4b**) are smaller than those of the phenylene-bridged analogues (**1** and **3**). The reduction in the HOMO–LUMO gap quantitatively accounts for the observed bathochromic shifts in the absorption spectra of the ethynylene-bridged derivatives.

4. Conclusions

In this study, four phosphine oxides incorporating anthryl and pyrenyl luminescent moieties were successfully synthesized: (4-(9-anthryl)phenyl)diphenylphosphine oxide (**1**), 9-anthrylethynyldiphenylphosphine oxide (**2**), (4-(1-pyrenyl)phenyl)diphenylphosphine oxide (**3**), and 1-pyrenylethynyldiphenylphosphine oxide (**4**). Recrystallization from various solvents afforded high-quality single crystals, and polymorphism was confirmed in the ethynylene-bridged derivatives bearing anthryl and pyrenyl groups. Consequently, six distinct crystalline structures were characterized across the four compounds. Photophysical investigations in both solution and solid states revealed that the ethynylene-bridged derivatives generally exhibited red-shifted absorption and emission relative to their phenylene-bridged counterparts, consistent with the enhanced resonance effect and extended π-conjugation introduced by the ethynyl linkage. Importantly, polymorphism was found to modulate the emission behavior. In particular, although the anthryl-containing compound **2** did not exhibit a substantial shift in emission maxima between its polymorphs, differences in vibrational stabilization were observed, leading to subtle variations in fluorescence features. These findings indicate that while the overall luminescence color remains largely unaffected by polymorphism, the vibrational states contributing to emission can be tuned through subtle modifications in molecular packing. Overall, this work demonstrates that weak intermolecular interactions and crystal polymorphism provide an additional level of control

over the excited-state dynamics of phosphine oxides. Furthermore, given that stimulus-induced structural transformations in the crystal lattice may also influence luminescence properties, the present results highlight the potential of crystal engineering as a strategy for the precise control of luminescence properties in organic functional materials.

Author contributions

All authors contributed to the preparation of the manuscript. All authors have read and approved the final version of the manuscript.

Conflicts of interest

The authors declare no conflicts of interest.

Data availability

All data supporting the findings of this study are provided in the supplementary information (SI).

Supplementary information is available. See DOI: https://doi.org/10.1039/d5ce00837a.

CCDC 2432548–2432553 (**1**, **2a**, **2b**, **3**, **4a** and **4b**) contain the supplementary crystallographic data for this paper.[20a–f]

Acknowledgements

The authors thank Dr. Okumura and Dr. Kawamura (Japan Synchrotron Radiation Research Institute, JASRI) for their invaluable assistance with X-ray data collection. The synchrotron radiation experiments were performed at the BL26B1 beamline of SPring-8 with the approval of JASRI (Proposal No. 2023B1221).

References

1 (*a*) Y. Qin, G. Li, T. Qi and H. Huang, *Mater. Chem. Front.*, 2020, **4**, 1554–1568; (*b*) Z. Wang, Q. Jingjing, X. Wang, Z. Zhang, Y. Chen, X. Huang and W. Huang, *Chem. Soc. Rev.*, 2018, **47**, 6128–6174; (*c*) H. Wang and D. H. Kim, *Chem. Soc. Rev.*, 2017, **46**, 5204–5236; (*d*) C.-T. Chen, *Chem. Mater.*, 2004, **16**, 4389–4400.

2 (*a*) Y. Wang, H. Wu, W. Hu and J. F. Stoddar, *Adv. Mater.*, 2022, **34**, 2105405; (*b*) Y. Lei, W. Dai, J. Guan, S. Guo, F. Ren, Y. Zhou, J. Shi, B. Tong, Z. Cai, J. Zheng and Y. Dong, *Angew. Chem., Int. Ed.*, 2020, **59**, 16054–16060; (*c*) S. Kundu, B. Sk, P. Pallavi, A. Giri and A. Patra, *Chem. – Eur. J.*, 2020, **26**, 5557–5582.

3 (*a*) X. Chen, T. Sun and F. Wang, *Chem. – Asian J.*, 2020, **15**, 21–33; (*b*) M. Tsurui, Y. Kitagawa, K. Fushimi, M. Gon, K. Tanaka and Y. Hasegawa, *Dalton Trans.*, 2020, **49**, 5352–5361; (*c*) S. V. Eliseeva and J.-C. G. Bünzli, *Chem. Soc. Rev.*, 2010, **39**, 189–227; (*d*) K. Binnemans, *Chem. Rev.*, 2009, **109**, 4283–4374; (*e*) A. de Bettencourt-Dias, *Dalton Trans.*, 2007, 2229–2241.

4 (*a*) Y. Hirai, T. Nakanishi and Y. Hasegawa, *J. Lumin.*, 2016, **170**, 801–807; (*b*) K. Miyata, Y. Konno, T. Nakanishi, A. Kobayashi, M. Kato, K. Fushimi and Y. Hasegawa, *Angew. Chem., Int. Ed.*, 2013, **52**, 6413–6416; (*c*) M. L. P. Reddy, V. Divya and R. Pavithran, *Dalton Trans.*, 2013, **42**, 15249–15262; (*d*) K. Miyata, T. Nakagawa, R. Kawakami, Y. Kita, K. Sugimoto, T. Nakashima, T. Harada, T. Kawai and Y. Hasegawa, *Chem. – Eur. J.*, 2011, **17**, 521–528; (*e*) K. Nakamura, Y. Hasegawa, H. Kawai, N. Yasuda, N. Kanehisa, Y. Kai, T. Nagamura, S. Yanagida and Y. Wada, *J. Phys. Chem. A*, 2007, **111**, 3029–3037; (*f*) Y. Hasegawa, M. Yamamuro, Y. Wada, N. Kanehisa, Y. Kai and S. Yanagida, *J. Phys. Chem. A*, 2003, **107**, 1697–1702.

5 (*a*) Y. Kitagawa, M. Tsurui and Y. Hasegawa, *RSC Adv.*, 2022, **12**, 810–821; (*b*) S. Miyazaki, K. Miyata, H. Sakamoto, F. Suzue, Y. Kitagawa, Y. Hasegawa and K. Onda, *J. Phys. Chem. A*, 2020, **124**, 6601–6606.

6 (*a*) C. Tang, X. Zhu, Y. Song, W. Liu, Q. Yang, Z. Lv and Y. Yang, *J. Photochem. Photobiol., A*, 2019, **376**, 263–268; (*b*) H. Ye, G. Liu, S. Liu, D. Casanova, X. Ye, X. Tao, Q. Zhang and Q. Xiong, *Angew. Chem., Int. Ed.*, 2018, **57**, 1928–1932.

7 (*a*) S. K. Rajagopal, P. S. Salini and M. Hariharan, *Cryst. Growth Des.*, 2016, **16**, 4567–4573; (*b*) L. Zou, X.-Y. Wang, K. Shi, J.-Y. Wang and J. Pei, *Org. Lett.*, 2013, **15**, 4378–4381.

8 (*a*) P. Ludwig, J. Mayer, L. Ahrens, F. Rominger, G. Ligorio, F. Hermerschmidt, E. J. W. List-Kratochvil, J. Freudenberg and U. H. F. Bunz, *Chem. – Eur. J.*, 2024, **30**, e202303037(1–8); (*b*) G. S. Baviera and P. M. Donate, *Beilstein J. Org. Chem.*, 2021, **17**, 2028–2050; (*c*) K. Kumar, K. K. Kesavan, D. Thakur, S. Banik, J. Jayakumar, C.-H. Cheng, J.-H. Jou and S. Ghosh, *ACS Omega*, 2021, **6**, 10515–10526; (*d*) M. Y. Lo, C. Zhen, M. Lauters, G. E. Jabbour and A. Sellinger, *J. Am. Chem. Soc.*, 2007, **129**, 5808–5809.

9 (*a*) I. Ahmad, S. J. Prathapa and A. A. Dar, *J. Mater. Chem. C*, 2025, **13**, 1161–11670; (*b*) A. A. Malik, Z. M. Saeed, I. Ahmad, T. Alkhidir, P. B. Managutti, S. Mohamed and A. A. Dar, *ACS Appl. Opt. Mater.*, 2024, **2**, 1709–1720; (*c*) A. A. Malik, A. A. Ganie, M. Wahid and A. A. Dar, *ACS Appl. Opt. Mater.*, 2024, **2**, 2229–2240; (*d*) A. A. Dar and A. A. Malik, *J. Mater. Chem. C*, 2024, **12**, 9888–9913; (*e*) A. A. Dar, A. A. Ahangar, C. Femina, A. A. Malik, J. V. Parambil and P. K. Sajith, *J. Phys. Chem. C*, 2024, **128**, 18901–18912; (*f*) G. Chakraborty, J. N. Malegaonkar, S. V. Bhosale, P. K. Singh and H. Pal, *J. Phys. Chem. B*, 2021, **125**, 11122–11133; (*g*) R. Liao, X. Wang, L. Peng, H. Sun and W. Huang, *ACS Appl. Mater. Interfaces*, 2021, **13**, 27491–27499; (*h*) C. Botta, S. Benedini, L. Carlucci, A. Forni, D. Marinotto, A. Nitti, D. Pasini, S. Righetto and E. Cariati, *J. Mater. Chem. C*, 2016, **4**, 2979–2989; (*i*) R. Hagihara, N. Harada, S. Karasawa and N. Koga, *CrystEngComm*, 2015, **17**, 8825–8834.

10 (*a*) J. Elguero, *Cryst. Growth Des.*, 2011, **11**, 4731–4738; (*b*) L. Yu, *Acc. Chem. Res.*, 2010, **43**, 1257–1266; (*c*) A. Nangia, *Acc. Chem. Res.*, 2008, **41**, 595–604; (*d*) W. I. F. David, K. Shankland, C. R. Pulham, N. Blagden, R. J. Davey and M. Song, *Angew. Chem., Int. Ed.*, 2005, **44**, 7032–7035.

11 (*a*) D. S. Reddy, D. C. Craig and G. R. Desiraju, *J. Am. Chem. Soc.*, 1996, **118**, 4090–4093; (*b*) D. S. Reddy, Y. E. Ovchinnikov, O. V. Shishkin, Y. T. Strychkov and G. R. Desiraju, *J. Am. Chem. Soc.*, 1996, **118**, 4085–4089.

12 (*a*) L. C. Gilday, S. W. Robinson, T. A. Barendt, M. J. Langton, B. R. Mullaney and P. D. Beer, *Chem. Rev.*, 2015, **115**, 7118–7195; (*b*) A. Mukherjee, *Cryst. Growth Des.*, 2015, **15**, 3076–3085; (*c*) T. M. Beale, M. G. Chdzinski, M. G. Sarwar and M. S. Taylor, *Chem. Soc. Rev.*, 2013, **42**, 1667–1680.

13 (*a*) S. Kikkawa, M. Takeno, T. Nakayama, D. Koike, Y. Saito, M. Tashiro, Y. Aoyama, H. Hikawa and I. Azumaya, *Cryst. Growth Des.*, 2024, **24**, 9564–9570; (*b*) S. Kikkawa, I. Maeno, K. Katagiri, Y. Murayama, M. Nozawa, H. Hikawa and I. Azumaya, *Cryst. Growth Des.*, 2021, **21**, 4380–4389; (*c*) S. Kikkawa, M. Okayasu, H. Hikawa and I. Azumaya, *Cryst. Growth Des.*, 2021, **21**, 1148–1158; (*d*) S. Kikkawa, H. Masu, K. Katagiri, M. Okayasu, K. Yamaguchi, H. Danjo, M. Kawahata, M. Tominaga, Y. Sei, H. Hikawa and I. Azumaya, *Cryst. Growth Des.*, 2019, **19**, 2936–2946.

14 *CrysAlis Pro version 171.39.20a*, Rigaku Oxford Diffraction, Tokyo, Japan, 2015.

15 O. V. Dolomanov, L. J. Bourthis, R. J. Gildea, J. A. K. Howard and H. Puschmann, OLEX2: a complete structure solution, refinement and analysis program, *J. Appl. Crystallogr.*, 2009, **42**, 339–341.

16 G. M. Scheldrick, *Acta Crystallogr., Sect. A: Found. Crystallogr.*, 2008, **64**, 112–122.

17 G. M. Scheldrick, *Acta Crystallogr., Sect. C: Struct. Chem.*, 2015, **71**, 3–8.

18 M. J. Frisch, G. W. Trucks, H. B. Schlegel, G. E. Scuseria, M. A. Robb and J. R. Cheesman, *Gaussian 09, Revision D.01*, Gaussian, Inc., Wallingford, CT, 2013.

19 (*a*) O. Tosic and J. Mattay, *Eur. J. Org. Chem.*, 2011, 371–376; (*b*) E. J. Corey and P. L. Fuchs, *Tetrahedron Lett.*, 1972, 3769–3772.

20 (*a*) CCDC 2432548: Experimental Crystal Structure Determination, 2026, DOI: 10.5517/ccdc.csd.cc2mn89w; (*b*) CCDC 2432549: Experimental Crystal Structure Determination, 2026, DOI: 10.5517/ccdc.csd.cc2mn8bx; (*c*) CCDC 2432550: Experimental Crystal Structure Determination, 2026, DOI: 10.5517/ccdc.csd.cc2mn8cy; (*d*) CCDC 2432551: Experimental Crystal Structure Determination, 2026, DOI: 10.5517/ccdc.csd.cc2mn8dz; (*e*) CCDC 2432552: Experimental Crystal Structure Determination, 2026, DOI: 10.5517/ccdc.csd.cc2mn8f0; (*f*) CCDC 2432553: Experimental Crystal Structure Determination, 2026, DOI: 10.5517/ccdc.csd.cc2mn8g1.